Nuclear Materials and Energy 12 (2017) 1348–1351

Contents lists available at ScienceDirect

Nuclear Materials and Energy

journal homepage: www.elsevier.com/locate/nme

Influence of the base temperature on the performance of tungsten under thermal and particle exposure

I. Steudel*, A. Huber, A. Kreter, J. Linke, G. Sergienko, B. Unterberg, M. Wirtz

Forschungszentrum Jülich GmbH, Institut für Energie- und Klimaforschung, 52425 Jülich, Germany

ARTICLE INFO

Article history:
Received 30 June 2016
Revised 23 January 2017
Accepted 9 March 2017
Available online 18 March 2017

ABSTRACT

Tungsten, the plasma facing material (PFM) for the divertor in ITER, must sustain severe, distinct loading conditions. This broad array of exposure conditions necessitates comprehensive experiments that cover most of the expected loading parameters to predict qualitative statements about the performance and as a consequence thereof the intended operation time. However, comprehensive experiments are inherently difficult to realize due to the fact that there is no device that is capable of simulating all loading conditions simultaneously. Nevertheless, the linear plasma device PSI-2 enables experiments combining thermal and particle exposure at the same time. In this work, sequential and simultaneous loads on pure tungsten at different base temperatures were investigated to study not only the performance of the material, but also the influence of the experimental parameters. The detailed analysis and comparison of the obtained results showed different kinds of damage depending on the loading sequence, power density, microstructure of the samples, and base temperature. Finally, samples with transversal grain orientation (T) showed the weakest damage resistance and the increase of the base temperature could not compensate the detrimental impact of deuterium.

1. Introduction

The expected conditions for the PFMs in ITER and especially for the most affected part, the divertor, are challenging. The PFMs and in-vessel components (PFCs) will be exposed to massive steady state heat loads, transient thermal events, and particle fluxes, which demand a great deal of the PFMs and PFCs in terms of performance, durability, and reasons of economy [1–4]. For this reason, comprehensive experiments are compulsory to predict performance and lifetime [5,6]. With regard to this necessity, simultaneous and sequential experiments were executed at the linear plasma device PSI-2 [7], located at Forschungszentrum Jülich. Double forged pure tungsten samples with diverse microstructures were investigated at different base temperatures (400 °C and 730 °C) under transient thermal (Nd: YAG laser) and steady state particle (deuterium plasma) loads. Moreover, not only the order of exposure was varied but also the power densities and pulse numbers. The purpose of these tests was to highlight potential influences of the loading conditions or combination of parameters on the damage behaviour and performance of the tested tungsten grade.

2. Experimental

The industrially available double forged pure tungsten (purity 99.97 wt%) [8], manufactured by Plansee SE Austria, was tested in the as-received and recrystallized state. For the preparation of recrystallized samples, samples with longitudinal grain orientation (L) were annealed for 1 h at 1600 °C. Afterwards, the microstructure was analysed to exclude influences from the pre-annealed microstructure. Samples with the dimension $12 \times 12 \times 5\,mm^3$ were cut by electrical discharge machining (EDM) and afterwards polished to a mirror finish to obtain a well-defined reference surface structure. From the as-received material, where the grains are disc-like shaped due to the forging during the manufacturing process, two different sample types were produced. On the one hand, samples with grains oriented parallel (longitudinal, L) to the loaded surface and on the other hand, samples with a perpendicular (transversal, T) orientation of the grains. Accessory, samples from the recrystallized tungsten (R) were produced. Hence, three different samples types (L, T, R) were tested under fusion relevant thermal shock conditions and particle exposure with varying loading sequences and at base temperatures of 400 °C and 730 °C. To specify, the thermal shock events were simulated by a Nd: YAG laser with a wave length of $\lambda = 1064\,nm$ and a maximum energy of 32 J at a pulse duration of 1 ms. The thermal loads, 100 and

* Corresponding author.
E-mail address: i.steudel@fz-juelich.de (I. Steudel).

http://dx.doi.org/10.1016/j.nme.2017.03.016

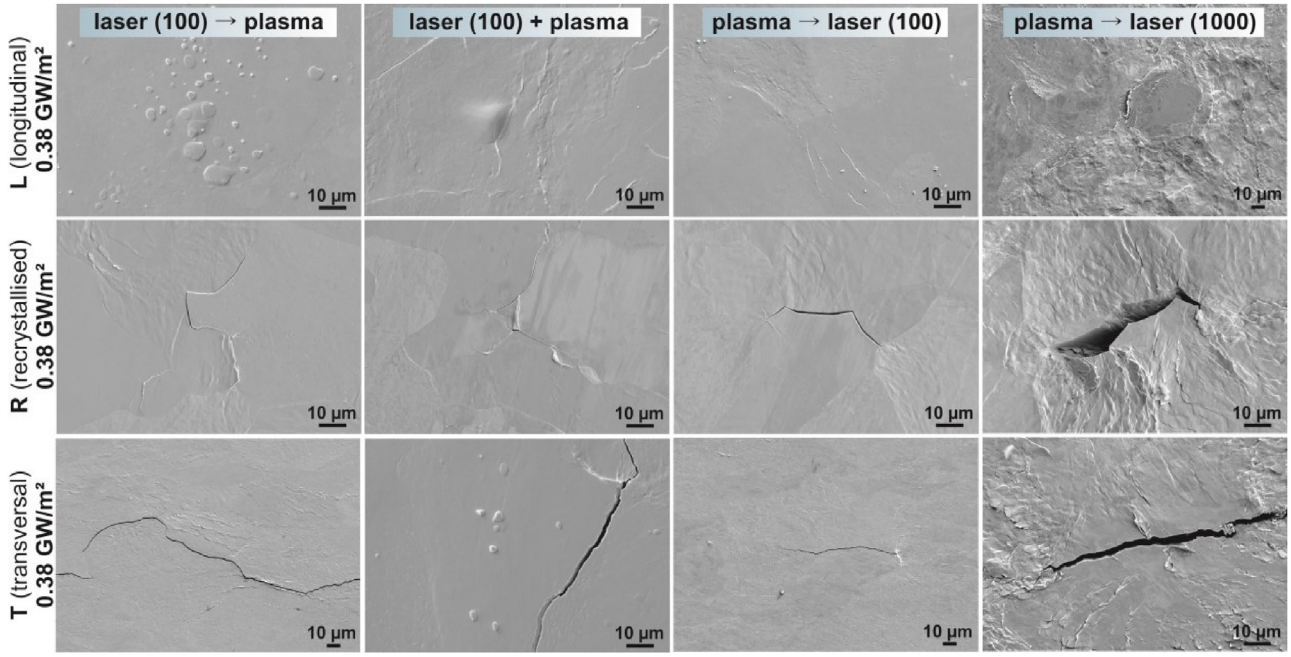

Fig. 1. SEM images of the exposed surfaces, in the top row of L followed by R and in the bottom row of T samples, after simultaneous and sequential test with a power density of 0.38 GW/m^2 at 400 °C. The highest surface roughness was observed after 1000 pulses (right column).

1000 pulses, had a repetition frequency of 0.5 Hz and the absorbed power densities covered a range of 0.19 GW/m^2 up to 0.76 GW/m^2. To determine the absorbed power density a laser power detector measured the laser energy, a photo diode was used to measure the reflection/transmission of all parts of the optical system, and a reflectometer measured the reflectance of the sample surface (~ 60%) [9]. This resulted in a laser absorption rate of 40% that was taken into account for the determination of the absorbed power densities. Furthermore, the particle exposure was realised by pure deuterium plasma with a plasma flux of 6×10^{21} m^{-2}s^{-1} and a fluence up to $1.2 \cdot 10^{25}$ m^{-2} (corresponding to 1000 laser pulses). At the same time, the particles were accelerated towards the sample by a bias voltage of –60 V, resulting in an incident ion energy of 35 eV. Moreover, an ohmic heater embedded in the sample holder ensured the achievement of the respective base temperature, which was monitored by a thermocouple. However, for each sample type (L,T,R) three samples, one for every defined absorbed power density (0.19 GW/m^2, 0.38 GW/m^2, 0.64 GW/m^2, 0.76 GW/m^2), were exposed. Only T samples were not tested with a power density of 0.19 GW/m^2 at 730 °C. Furthermore, the loading sequence was changed from spot-to-spot so that at the end each sample hold four different exposure spots. More precisely, the first spot (1) was loaded with 100 laser pulses followed by plasma exposure. At the second spot (2) the loading was simultaneous, whereas the third (3) and fourth (4) spot were primarily encountered by the plasma and successively by 100 and 1000 laser pulses, respectively. This loading method provides the opportunity to simultaneously study a set of effects and correlations of/between the experimental parameters and performance of tungsten. Afterwards, the generated modifications and damages were analysed by laser profilometry, light microscopy, scanning electron microscopy (SEM) and metallographic cross sections.

3. Results and discussion

To start a self-contained discussion and comparison of the influence of different base temperatures on the performance of tungsten, the results of experiments at 400 °C base temperature, already published in [10], will shortly be summarised herein. Fig. 1 illustrates exemplary SEM images of loaded surfaces after experiments at 0.38 GW/m^2 for all sample types.

At 400 °C the order of exposure had a substantial impact on the surface morphology, which was reflected on blister formation (Fig. 1). At 0.38 GW/m^2 the sequence, which ended with plasma exposure, evoked a considerable amount of blisters within the loaded area. Here, deformed samples (L, T) showed a higher content of blisters than recrystallized samples (R), which can be traced back to the higher amount of existing defects (i.e. dislocations, grain boundaries) in deformed samples caused by the manufacturing process, microstructure etc. that acted as trapping sites for H [11,12]. Moreover, the preceding exposure to thermal shock loads caused additional defects, in which H could accumulate, as stated in [13]. For all other loading orders at lower/higher power densities the amount of blisters diminished to the point of no blisters.

Furthermore, it was found that the adverse impact of H exacerbated the damage behaviour and performance substantially. This exacerbation, H embrittlement, was reflected in crack emergence on T and R samples independent of the loading sequence. The accumulated H in combination with stresses generated by transient events prevented the stress relieve of T and R samples just by plastic deformation. In contrast, L samples benefited from texture strengthening effects, higher fracture strain and yield strength, and did not show cracks at all. Moreover, metallographic cross section analysis revealed that the cracks of T samples propagated primarily perpendicular to the loaded surface and along the grain boundaries, whereas R samples cracked perpendicular and horizontal. Especially, the formation of horizontal cracks entails the risk of overheating, melting, and material loss and, therefore, abridges the lifetime of PFMs and compromises the impeccable operation of a fusion device. The number of detectable cracks on metallographic cross sections varied between 1 and 10, which produced a poor statistic but depicted that with rising power densities the crack depth increased. Therefore, T samples generated the deepest cracks after tests at 0.64 GW/m^2. Here, two cracks were observed after initial laser loading followed by plasma exposure with an average crack depth of ~ 394 µm ± 191 µm. Metallographic cross sec-

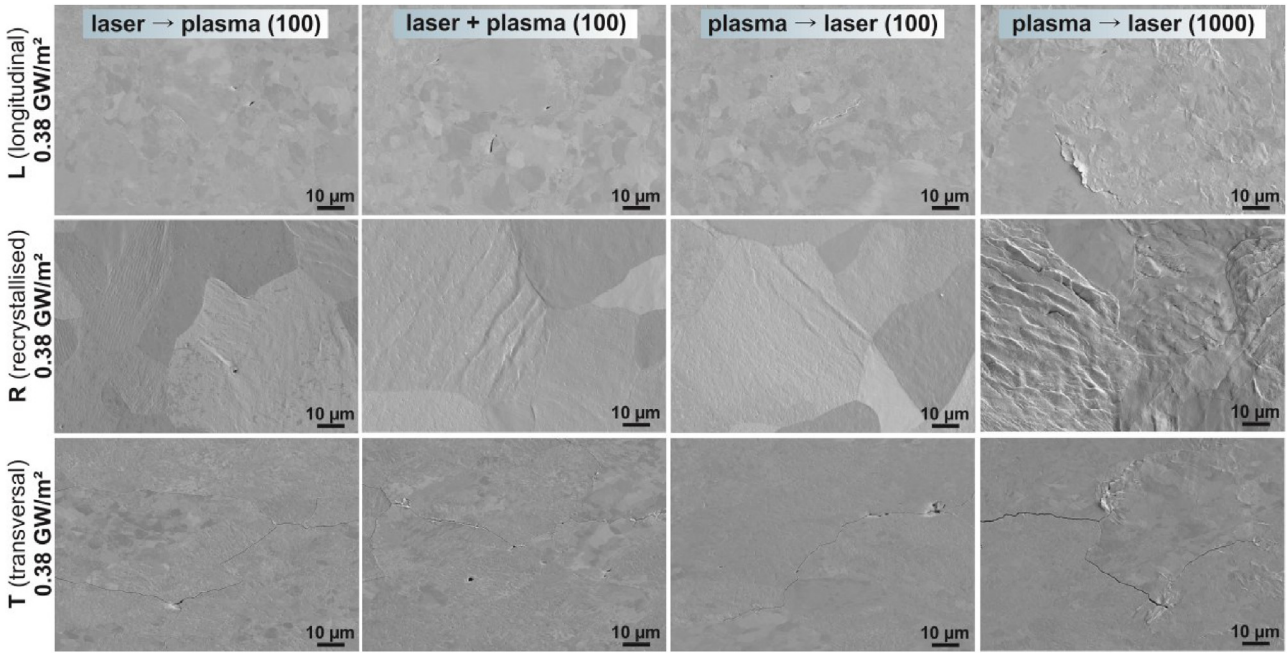

Fig. 2. Exemplary SEM images of the loaded surfaces after tests at 730 °C with a power density of 0.38 GW/m^2. The top row illustrates examples of L sample surfaces succeed by R samples and in the bottom row T samples. The sequence with 1000 laser pulses led to pronounced roughening.

tions revealed that the deepest cracks on R samples were found after tests at 0.38 GW/m^2. The measured average crack depth was 106 µm ± 104 µm.

To investigate if the base temperature measurably influences the performance or mitigates the exacerbating impact of deuterium, subsequent tests were conducted at 730 °C while all other loading requirements were maintained. In Fig. 2, SEM images of exposed surfaces of all sample types are shown.

Experiments at a base temperature of 730 °C exhibited that the damage threshold for all sample types shifted below 0.19 GW/m^2, which was mainly reasoned by the temperature rise that decreased the mechanical properties and H embrittlement that also acted opposing the gain in ductility. Furthermore, for none of the sample types blisters were observed. This was on the one hand traced back to microstructural changes (i.e. grain nucleation), which were detected on metallographic cross sections and evoked by the elevated base temperature. Amongst other, these microstructural changes reduced the number of existing trapping sites for H [11]. On the other hand and as stated in [14–16], by rising the base temperature the number of blisters decreases due to the temperature dependence of H retention. Simultaneously, the amount of out-gassing hydrogen increases. This increase of out-gassing H was reflected in the formation of pores/cavities that were arbitrarily distributed in the loaded area but numerously represented on single grains. Due to the fact that blistering preferentially occurs on grains with lattice orientation (111) [11], this could also be an explanation for the distribution of the pores/cavities. Further investigations are required to confirm the result. However, a direct correlation between the loading sequence and the pores/cavities was not descried, certainly there seemed to be a slight interrelation between power density and pulse number. Fig. 3 depicts damage mappings for both tested base temperatures and all sample types as well as exposure sequences.

In addition to the afore referred results, the thermal shock behaviour of L samples remained unchanged, with the exception that laser subsequently plasma exposure at 0.76 GW/m^2 generated small cracks within the loaded area. These small cracks were extremely shallow and therefore, not visible on metallographic cross sections.

The effect of the temperature rise on R samples became apparent by the absence of cracks. Here, the gain in ductility could have balanced the weaker mechanical properties due to the recrystallized microstructure. Only power density and pulse number dependent surface roughening was observed, accessorily pores/cavities and microstructural changes, as already mentioned. In general, pores/cavities were least developed on R samples. The same was observed for experiments at 400 °C concerning blister formation. A reason for the reduced blister formation was the recrystallised microstructure itself because recrystallization eliminates not only dislocations but also vacancies and/or vacancy clusters [11,17]. This in turn degrades the trapping sites for hydrogen and, therefore, appeared to be the reason that less pores/cavities were monitored after tests at 730 °C.

T samples showed the weakest damage resistance. In comparison with tests at 400 °C, the performance dropped, which became apparent by crack and crack network formation under virtually any loading scenario. This fact evidenced the autonomy of thermal shock behaviour and loading order and the significant effect of the microstructure and H embrittlement. Considering that a higher base temperature should increase the ductility so that the stresses are relieved by plastic deformation, the brittle behaviour of T samples indicated that this expectation was not met in this case. This outcome is critical, since the transversal grain orientation is the preferential orientation for applications in ITER.

Furthermore, by elevating the applied power density and pulse number, not only the surface roughness rose as it was detected for all sample types, but also the crack depth. Metallographic cross sections disclosed that the cracks, generated at 0.38 GW/m^2, had an exceedingly shallow penetration depth. Owing to this, only six cracks after 1000 laser pulses could be discovered with an average crack depth of ~ 16 µm ± 10 µm. After experiments at 0.76 GW/m^2 the deepest cracks were measured for the loading sequence with initial plasma exposure followed by 100 transient events. Here, the average crack depth was 43 µm ± 59 µm and the deepest crack had a depth of ~ 220 µm ± 10 µm. Additionally, this crack was accom-

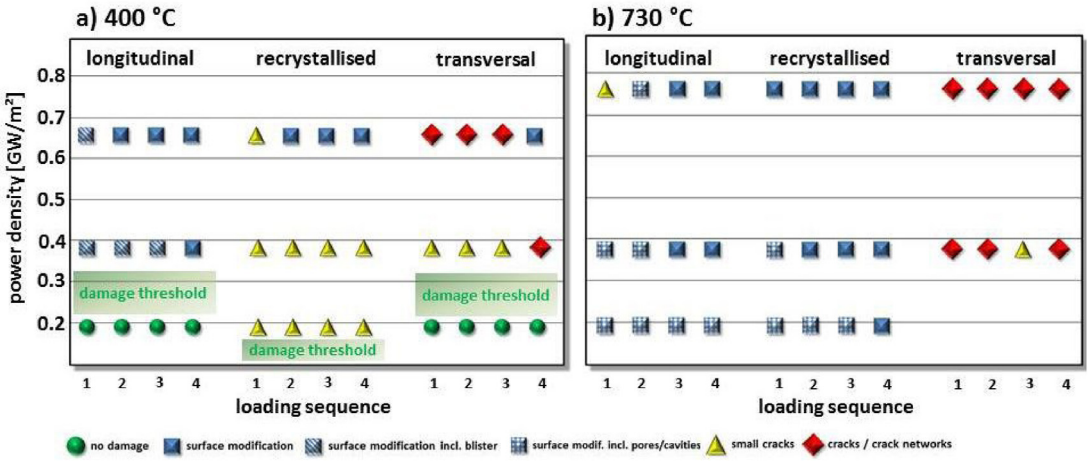

Fig. 3. Damage mappings of the described tests as a function of the loading sequence and absorbed power density. The left graph illustrates the results for experiments at 400 °C, the right graph at 730 °C. Furthermore, the 400 °C graph contains damage thresholds for all tested samples types that became apparent.

panied by cracks that generated within the material in a depth of 130 µm ± 10 µm. Such cracks are especially detrimental because they are not detectable on the surface.

In general, the metallographic cross sections identified that the cracks propagated almost along the grain boundaries perpendicular to the loaded surface into the material.

4. Conclusion

The comparison of the obtained results showed that at 400 °C base temperature, there was a clear correlation between applied power densities, pulse number, and damage behaviour, whereas at 730 °C base temperature this correlation was not obvious with the exception of the surface roughness. This result could be traced back to the higher ductility of tungsten. Nevertheless, there is a potential connection between the occurrence/number of pores/cavities and the applied power density due to a determined difference in the amount. At low power densities, the number appears to be higher, which could be explained by a lower mobility of hydrogen and, therefore, more agglomeration in the surface-near region. Consequently, the stresses inside the material are larger, which in turn results in enhanced erosion effects. This assumption will be pursued in future tests.

Apart from that, blisters, whose amount was heavily dependent on the order of loading, were only observed for experiments at 400 °C. However, the exacerbating effect (embrittlement) of deuterium on the material performance was detected in both test series not least by the formation of cracks and crack networks.

Moreover, experiments at 730 °C caused significant grain nucleation up to several 10 µm deep independent of loading sequence, power density, and pulse number. This nucleation will lead to a recrystallized microstructure and, therefore, degrade the mechanical properties of the material. Texture strengthening effects attributed to the as received microstructure, as it became apparent in the case of L samples, would slowly disappear and already mechanically weak materials would degrade even more [18]. With regard to an application in a fusion device like ITER, this could have severe influences on a frictionless operation and the lifetime of the components. Especially, the weak damage resistance of the transversal grain orientation, which is the favoured orientation for applications in ITER, could possibly provoke problems.

Nevertheless, it can neither be claimed nor be evidenced that an increase of the base temperature improved the material performance or compensated the adverse impact of deuterium, albeit some sample types did not show an apparent deterioration of the performance.

Supplementary materials

Supplementary material associated with this article can be found, in the online version, at doi:10.1016/j.nme.2017.03.016.

References

[1] H. Bolt, et al., J. Nucl. Mater. 307-311 (2002) 43–52.
[2] G. Federici, J. Nucl. Mater. 337-339 (2005) 684–690.
[3] ITER Physics Basis Editors, et al., Nucl. Fusion 39 (1999) 2137–2174.
[4] M. Rieth, et al., J. Nucl. Mater. 432 (2014) 482–500.
[5] M. Wirtz, et al., J. Nucl. Mater. 420 (2012) 218–221.
[6] G. Pintsuk, in: Comprehensive Nuclear Materials, Elsevier, 2012, pp. 551–581.
[7] A. Kreter, et al., Fusion Sci. Technol. 68 (2015) 8–14.
[8] G. Pintsuk, et al., J. Nucl. Mater. 417 (2011) 481–486.
[9] M. Wirtz, et al., J. Nucl. Fusion 55 (2015) 123017.
[10] I. Steudel, Phys. Scripta T167 (2016) 014053.
[11] D. Terentyev, et al., J. Nucl. Fusion 55 (2015) 013007.
[12] O.V. Ogorodnikova, et al., J. Appl. Phys. 103 (2008) 034902.
[13] A. Huber, et al., Phys. Scripta T167 (2016) 014046.
[14] C. García-Rosales, J. Nucl. Mater. 233-237 (1996) 803–808.
[15] O.V. Ogorodnikova, J. Nucl. Mater. 313-316 (2003) 469–477.
[16] G.-N. Luo, et al., Fusion Eng. Des. 81 (2006) 957–962.
[17] H. Eleveld, J. Nucl. Mater. 212-215 B (1994) 1421–1425.
[18] M. Wirtz, et al., Fusion Eng. Des. 9-10 (2013) 1768–1772.